



HAL
open science

The Mw 7.5 1999 Ambrym earthquake, Vanuatu: a back arc intraplate thrust event

Marc Regnier, Stéphane Calmant, Bernard Pelletier, Yves Lagabrielle, Guy Cabioch

► To cite this version:

Marc Regnier, Stéphane Calmant, Bernard Pelletier, Yves Lagabrielle, Guy Cabioch. The Mw 7.5 1999 Ambrym earthquake, Vanuatu: a back arc intraplate thrust event. *Tectonics*, 2003, 22 (4), pp.1034. 10.1029/2002TC001422 . hal-00407047

HAL Id: hal-00407047

<https://hal.science/hal-00407047>

Submitted on 28 Jan 2021

HAL is a multi-disciplinary open access archive for the deposit and dissemination of scientific research documents, whether they are published or not. The documents may come from teaching and research institutions in France or abroad, or from public or private research centers.

L'archive ouverte pluridisciplinaire **HAL**, est destinée au dépôt et à la diffusion de documents scientifiques de niveau recherche, publiés ou non, émanant des établissements d'enseignement et de recherche français ou étrangers, des laboratoires publics ou privés.

The M_w 7.5 1999 Ambrym earthquake, Vanuatu: A back arc intraplate thrust event

Marc Regnier, Stéphane Calmant, Bernard Pelletier, and Yves Lagabrielle

UR082/UMR Géosciences Azur, Institut de Recherche pour le Développement, Nouméa, New Caledonia

Guy Cabioch

UR055 "Paléotropique", IRD, Nouméa, New Caledonia

Received 30 May 2002; revised 28 November 2002; accepted 4 April 2003; published 26 July 2003.

[1] On 26 November 1999, a M_w 7.5 thrust earthquake occurred in the Vanuatu back arc seismic zone. The aftershocks seismicity defines a west dipping plane down to a depth of 20 km consistent with the focal mechanism geometry. The shallow focal depth of the main shock and the coincidence of the surface projection of the plane of aftershocks with a 600 m high sea bottom fault scarp indicate the fault plane ruptured up to the surface. The size of the fault has been estimated to 50×25 km² from the aftershocks distribution and modeling of coseismic vertical motion inferred from biological markers. The inferred length indicates the rupture affected the whole Ambrym segment, but inversion of GPS horizontal displacement data indicates most of the seismic moment has been released on a smaller 35×20 km² fault surface with an average slip of 6.5 m. Foreshock and aftershock seismicity are organized in planar seismic zones parallel to the inferred main shock rupture plane. This spatiotemporal distribution of imaged fault suggests that the thrust front propagates in times by eastward jumps to new intraplate faults occurring in the western edge of the North Fiji Basin. The back arc present setting could eventually represent the very early stages of an incipient subduction zone with reverse polarity. The intraplate fault model yields shortening by thickening of the back arc crust. Using crustal balanced sections to model the deformations over the last 1.8 m.y. period, a maximum shortening of 55 km has been found

INDEX TERMS: 1242 Geodesy and Gravity: Seismic deformations (7205); 1206 Geodesy and Gravity: Crustal movements—interplate (8155); 7215 Seismology: Earthquake parameters; 7230 Seismology: Seismicity and seismotectonics; 7220 Seismology: Oceanic crust; *KEYWORDS:* seismotectonics, subduction zone, back arc, thrust fault, intraplate.

Citation: Regnier, M., S. Calmant, B. Pelletier, Y. Lagabrielle, and G. Cabioch, The M_w 7.5 1999 Ambrym earthquake, Vanuatu:

A back arc intraplate thrust event, *Tectonics*, 22(4), 1034, doi:10.1029/2002TC001422, 2003.

1. Introduction

[2] The large earthquake (M_w 7.5) that occurred in Central Vanuatu on 26 November 1999 was the most damaging event to strike in Vanuatu since the M_w 7.1 October 1971 Santo event. It triggered a tsunami observed on all neighboring islands, caused the death of 10 peoples and extensive damages to buildings and infrastructures. It is also the largest known thrust fault earthquake in this part of the New Hebrides island arc characterized by the subduction-collision of the d'Entrecasteaux Ridge. This segment is composed, across strike, of two island thrust belts bracketing the deep intraarc Aoba basin (Figure 1). The main shock epicenter (latitude 16.188°S, longitude 168.288°E, and depth 14 km) was located in the southern part of the back arc belt of the central segment of Vanuatu, east of Ambrym island. Such a large thrust event is normally expected to occur in the forearc domain, along the plate boundary to accommodate the convergence motion. The fault on which the Ambrym earthquake occurred is part of a system of north-south trending back arc faults [Collot *et al.*, 1985; Pelletier *et al.*, 1994]. The comparable seismic activity and convergence rate along the western and eastern belts [Taylor *et al.*, 1995; Calmant *et al.*, 1995; Pelletier *et al.*, 1998] suggest they both undergo high deformations to accommodate together the average regional convergence rate of 9 cm/yr. While the shortening along the western belt is thought to be (at least partly) accommodated by a motion of subduction beneath the New Hebrides arc, the mode of convergence along the eastern belt is not known. Convergence can be achieved by either subduction or crustal thickening. In each case, one expects different earthquakes distributions and thrust belt morphologies. So far, poor earthquake locations from global or regional catalogues do not provide the data to address this issue.

[3] The analysis of the November 1999 Ambrym earthquake sequence recorded locally allows us to better resolve the back arc fault system and to bring some new constraints on the mode of shortening along the back arc belt. The spatial distribution of the aftershocks, together with GPS data and field observations of the coseismic displacements recorded right after the earthquake, are used to estimate the

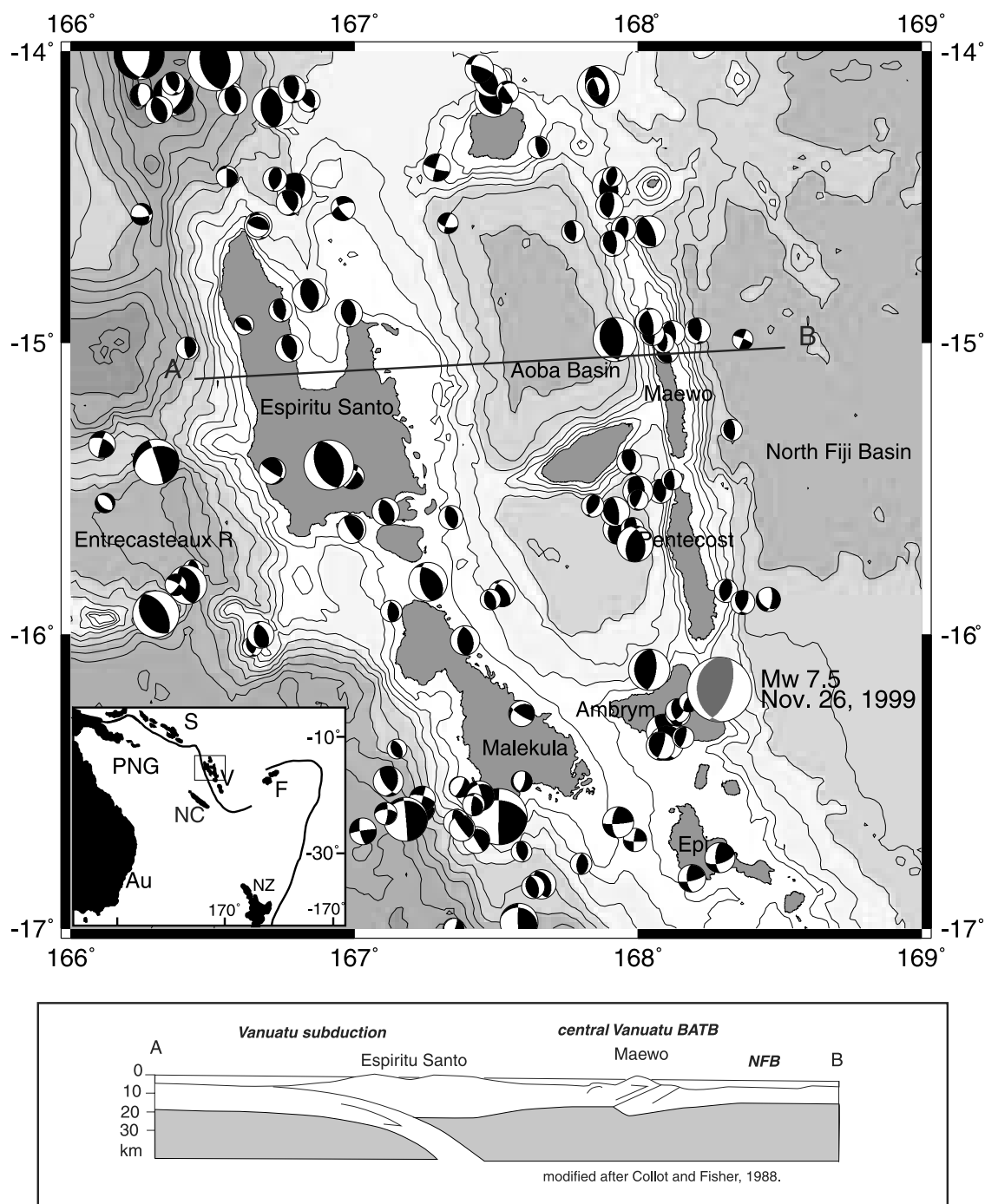


Figure 1. (top) Shallow seismicity of the central Vanuatu region. Only the events with a CMT solutions are reported (location NEIC) for the period 1977–2001. The position of the 26 November 1999 Ambrym event is from the local ORSTOM-IRD Network, its solution being from CMTS. Note that the BATB front is characterized by pure compressive events. Inset shows the location of study area in southwest Pacific; A, Australia; F, Fiji; NC, New Caledonia; NZ, New Zealand; PNG, Papua New Guinea; S, Solomon; V, Vanuatu. (bottom) simplified structural section (AB) across the arc subduction and the back arc thrust belt (BATB) of central Vanuatu. Section AB is modified from an original section by Collot and Fisher [1989].

spatial extend of the rupture zone. Main fault characteristics and comparison of earthquakes distribution before and during the sequence allow arguing that the earthquake sequence is related to an oceanic intraplate west dipping thrust fault system rather than to a steady interplate boundary-type setting. We will also show that the static stress changes caused by our inferred fault model can explain the main patterns of the aftershocks sequence.

2. Tectonic Setting

[4] The subduction process in the central part of the arc of Vanuatu is heavily perturbed by the d'Entrecasteaux aseismic ridge which is located on the subducting Australian plate and trends roughly perpendicular to the trench [Collot *et al.*, 1985]. This causes the interplate thrust zone to be partly locked up and the central segment to be shoved eastward [Taylor *et al.*, 1995], creating a back arc compressional zone. Seismicity and neotectonic studies [Taylor *et al.*, 1987; Louat and Pelletier, 1989] show an uplift of both western and eastern belts and active shallow thrust zones in both the forearc and back arc domains. The most recent and complete GPS study [Calmant *et al.*, 2003] indicate a 5–6 cm/yr of convergence rate along the eastern belt boundary in the $N87^\circ$ direction (at the Ambrym latitude) and a 3.5–4 cm/yr convergence rate at the western plate boundary in the $N70^\circ$ direction. These values indicate an even higher rate of convergence along the back arc thrust belt (BATB) than along the plate boundary. Refraction and gravity studies [Collot and Fisher, 1989; Pontoise *et al.*, 1994] show a similar crustal structure of the oceanic crust on both sides of the eastern belt and an asymmetrical dense crustal root beneath it. This is interpreted as an underthrust of the North Fiji Basin (NFB) beneath the BATB.

[5] The November 1999 Ambrym earthquake occurred in the southern part of the back arc thrust zone. The focal mechanism solution published by Harvard (CMTS) indicates the event has a dominantly thrust mechanism. Considering the tectonics of central Vanuatu and the permanent shallow seismicity of the eastern belt characterized by west dipping patterns, the fault plane striking at 174° and dipping westward at 30° is interpreted to be the fault plane.

[6] Although the Ambrym earthquake CMTS is compatible with the mechanisms of the medium size earthquakes located along the BATB (Figure 1), its significant strike-slip component (rake of 67°) yields a motion in $N110^\circ$ direction of the hanging block, while an eastward motion is expected from the relative plate convergence direction [Calmant *et al.*, 2003]. This large difference is consistent with a non uniform stress field along the BATB as first pointed out by Louat and Pelletier [1989] from the analysis of CMTS P axis strike variations along the belt. Focal mechanisms of shallow earthquakes from the Harvard catalogue are plotted on the Figure 1. They gather in small groups around the terminations of islands of the BATB with an average spacing between groups of 40–50 km equal to the islands average length. This earthquake distribution defines a succession of gaps and clusters, in between islands, along

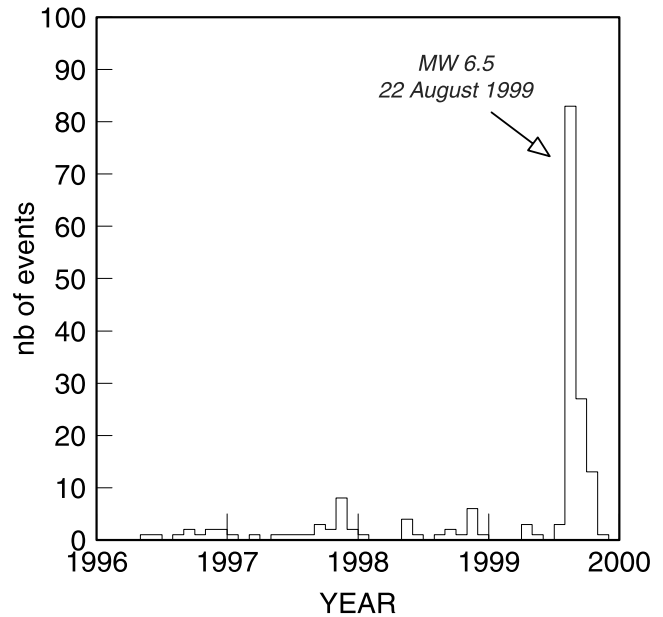


Figure 2. Histogram of the seismic activity in the Ambrym segment during the 3 years preceding the 26 November 1999 main shock. The pick of activity in the second half of 1999 is related to a M_w 6.5 earthquake that occurred in the fault system of the main shock. It is considered as a foreshock swarm.

the belt. This seismic pattern together with the discontinuous morphology of the eastern belt strongly suggests the BATB is along strike segmented, probably as the result of the non uniform stress field, and that each island materializes a locked segment with some permanent seismic activity between them. The southernmost segment of the BATB is centered on Ambrym island. It stretches from the southern end of Pentecost island to south of Ambrym island where the southernmost cluster of back arc thrust faulting activity can be observed (Figure 1). The 26 November 1999 earthquake occurred in the middle of this segment. Some seismic activity occurred within the Ambrym segment during 1999 (Figure 2). The increase of the activity in 1999 is essentially due to a medium size shallow thrust earthquake (M_w 6.5) that took place on 22 August 1999 in the same area (latitude $16.117^\circ S$, longitude $168.039^\circ E$, NEIC) than the 26 November 1999 earthquake. Unfortunately, because of a power failure that day, the 22 August earthquake was not recorded by the network so we cannot provide our own location for this event. The sequence that followed the 22 August event, located by the local network, defines a zone of seismicity located immediately to the north of the 26 November epicenter, within the Ambrym segment. Its focal solution (CMTS from Harvard) is a pure thrust-type mechanism showing east-west compression. As for the November 1999 Ambrym earthquake, the plane striking at 179° and dipping westward at 28° is interpreted as the fault plane. Because of its same location and fault plane geometry, the 22 August event sequence appears to be part of the fault system active during the 26 November

Table 1. Velocity Structure Used Under the Stations in the Location Process^a

Depth, km	<i>P</i> Velocity, km/s
<i>Stations on the Western Belt</i>	
0	2.40
2	6.40
17	8.10
<i>Stations on the Eastern Belt</i>	
0	2.40
2.5	6.50
20	8.00

^aThe model for the station on the western belt has a faster upper mantle velocity and a thinner crustal thickness to account for the propagation through the oceanic Aoba basin.

earthquake. This sequence is then considered as a foreshocks swarm of the main shock.

3. Seismic Sequence Location

[7] The earthquake locations presented here are from data recorded by the IRD permanent seismic network in Vanuatu [Regnier *et al.*, 2001]. The network consists of nine three-component stations equipped with 1 Hz short-period sensor or broadband CMG3 seismometers. The three broadband stations have a 24 bits continuous recording stand alone acquisition while the short-period stations use FM telemetry to transmit data to a central recording site working in trigger mode. All stations use GPS clocks. A major difficulty in locating earthquakes in the back arc region is that the seismic area lies on one side of the local network. In addition, the velocity structure in the region is highly heterogeneous. Ray paths from hypocenters in the back arc region can sample different structures such as oceanic basins, volcanic areas and old island arc belts. The major lateral velocity contrast is probably across the Aoba basin which has been characterized as an oceanic basin with a crustal structure very similar to that of the NFB [Pontoise *et al.*, 1994]. To partially overcome this heterogeneous velocity structure problem, we used a different model to compute travel time to each station for locating earthquakes. In particular, to compute travel times to stations on the western belt, a simplified oceanic like velocity model [Pontoise *et al.*, 1994] has been used (Table 1) to account for the propagation through the Aoba Basin. We also used a nonlinear grid search locating process in which the whole space is sampled to find the smallest rms. We only present locations computed with *P* and *S* waves readings from at least five stations. For all the computed locations, the average RMS is 0.087 s. Estimated errors on the epicenter are of the order of few kilometers. Uncertainty on the depth is 5 km.

4. Main Shock

[8] On the basis of local travel times, the main shock was located at -16.188°S , 168.288°E with a depth of 14 km. The broadband analysis of this event by Harvard results in a

Table 2. Main Shock Locations and Focal Mechanism Solutions

Organization	Longitude, deg	Latitude, deg	Depth, km	Strike, deg	Dip, deg	Rake, deg	M_0 , N m ($\times 10^{20}$)
IRD	168.288	-16.188	14	170	40	60	1.67
NEIC	168.210	-16.420	33	150	23	48	0.93
HRV	168.310	-16.080	15	174	30	67	1.67

depth of 15 km (fixed) and an epicenter located 13 km northeastward. USGS location puts the epicenter 25 km further south (see Table 2), which appears inconsistent with local data. The Harvard CMTS for this event is not a good one according to Frohlich's criteria [Frohlich *et al.*, 1997], mainly because the number of constrained moment tensor elements is 4, that is, their error is set to zero ($n_{\text{free}} = 2$). The computation of the relative error on the moment tensor (MT) and of its nondouble-couple component is then irrelevant. With regional data, the source duration has been estimated to 50 s and the source time function appears to be made up of four distinct periods of moment release well separated in time [Pillet *et al.*, 2000]. The main shock epicenter is located roughly in the middle of the Ambrym seismic zone, suggesting a bilateral rupture. This source model is also supported by the closeness of the first motion and centroid locations [Smith and Ekstrom, 1997]. Both the complexity of the source revealed by its time history [Pillet *et al.*, 2000] and the possibility of the variation of focal mechanism during the rupture are likely the causes of the difficulty of the MT determination [Kikuchi and Kanamori, 1991]. Studies of the source of the main shock using EGF techniques and body wave inversion [Nabelek, 1984] will be described in other works. The Harvard and USGS focal mechanisms have been checked with first motion data from the local IRD network. Our first motion solution differs slightly from the two CMT solutions (Figure 3 and Table 2). Only the strike and dip of the interpreted fault plane have been further constrained with our data. The strike of the inferred fault plane (170°) more closely parallels the general

26/11/1999 13:21

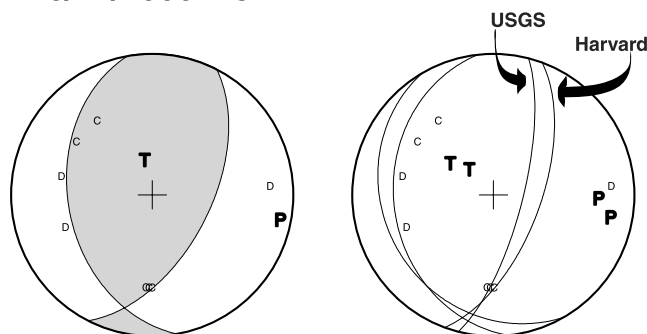


Figure 3. (left) First-motion focal mechanism solution of the 26 November 1999 Ambrym earthquake obtained with local data. (right) Harvard and USGS solutions together. Some polarities (dilatations) are incompatible with both solutions, suggesting a steeper fault (40°) plane at the nucleation of the main shock.

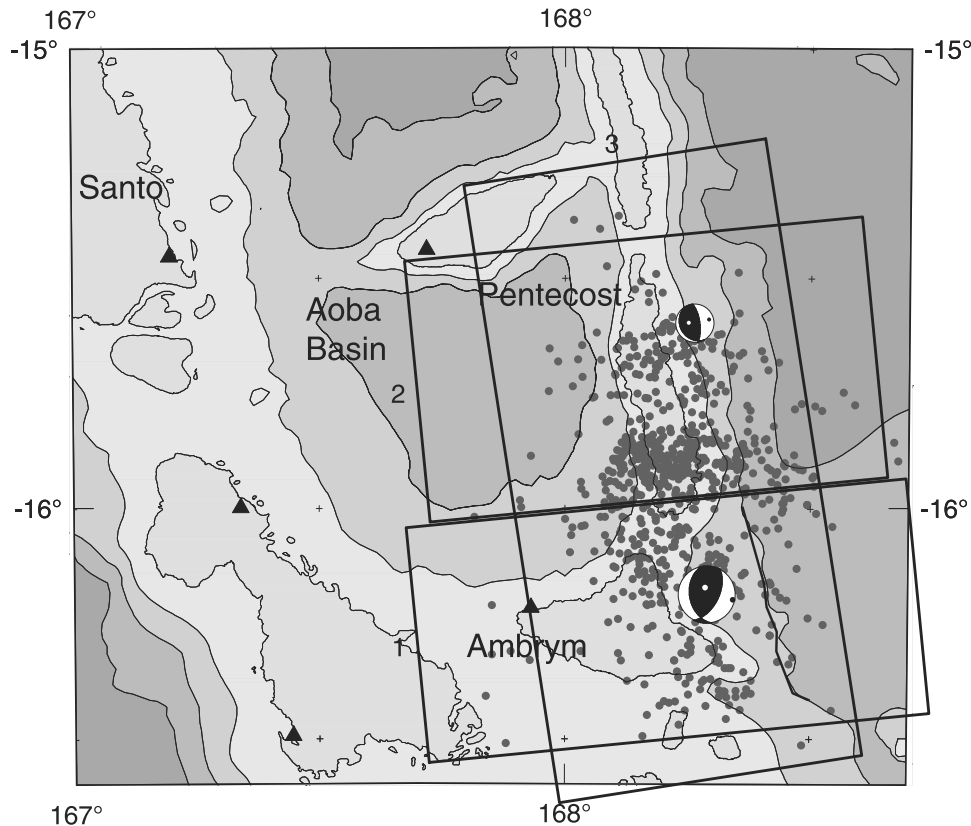


Figure 4. Map of shallow epicenters (depth < 30 km) for a 7 month period after the main shock. The locations of the cross sections are reported. The mapped seafloor scarp is plotted as a black line east of the main shock around the isobaths 2000 m. See color version of this figure at back of this issue.

trend of the eastern belt (N165°, Figure 4). The major change is in the dip angle of the fault plane that goes from 30° to 40°. The differences between the solutions might reflect the variation of mechanism during the rupture that is taken into account by the centroid solutions. The surface projection of the fault plane is very close to a large sea bottom mapped fault scarp (Y. Lagabrielle et al., Coseismic and long-term vertical displacement due to back arc shortening, central Vanuatu: An integrated analysis of field and marine data following the M_w 7.5, 26 November 1999, Ambrym earthquake, submitted to *J. Geophys. Res.*, 2003, hereinafter referred to as Lagabrielle et al., submitted manuscript, 2003) that lies in the NFB, east of Ambrym island (Figure 4), at a depth of 2000 m and trending N165° as the eastern belt. Considering its right position with respect to the main shock focus and its simple linear geometry with the west side uplifted, the mapped fault scarp is likely to be the surface expression of the M_w 7.5 earthquake. Together with the shallow depth of the event it implies that the rupture reached the surface and helped out creating the large deadly tsunami.

5. Aftershocks Distribution

[9] The aftershocks span an area of about $80 \times 30 \text{ km}^2$ [Pelletier et al., 2000] with the largest concentration to the

north of the main shock hypocenter. The whole aftershock zone has been active immediately after the main shock and no spatiotemporal seismic pattern has been recognized. Among the thousands aftershocks recorded, we were able to locate with accuracy 920 events. Three zones of aftershock activity are identified on map view (Figure 4): the zone of Ambrym Island, where the main shock occurred, characterized by a relatively low level of activity, and two smaller zones along Pentecost Island characterized by denser clusters of earthquakes.

[10] In cross sections 1 and 2 (Figure 5, location on Figure 4), oriented perpendicular to the fault plane, the seismicity resolves in a broad west dipping zone imaging the thrust fault determined from the CMTS. In section 1, where the main shock occurred, the dip of one of the seismic zone is about the same than the dip of one the planes of the CMTS (30°) and its surface projection coincides with the location of the sea bottom mapped fault scarp. The low level of aftershock activity in this zone probably indicates the location of the rupture area where most of the accumulated stresses has been released. Farther north, in section 2, the jigsaw pattern of the upper limit of the seismicity suggests the aftershock seismic activity occurred on several faults, eventually sub parallel to the dipping lower limit of the cluster.

[11] In section 3, roughly N-S oriented and parallel to the average trend of the eastern belt, the two major features are

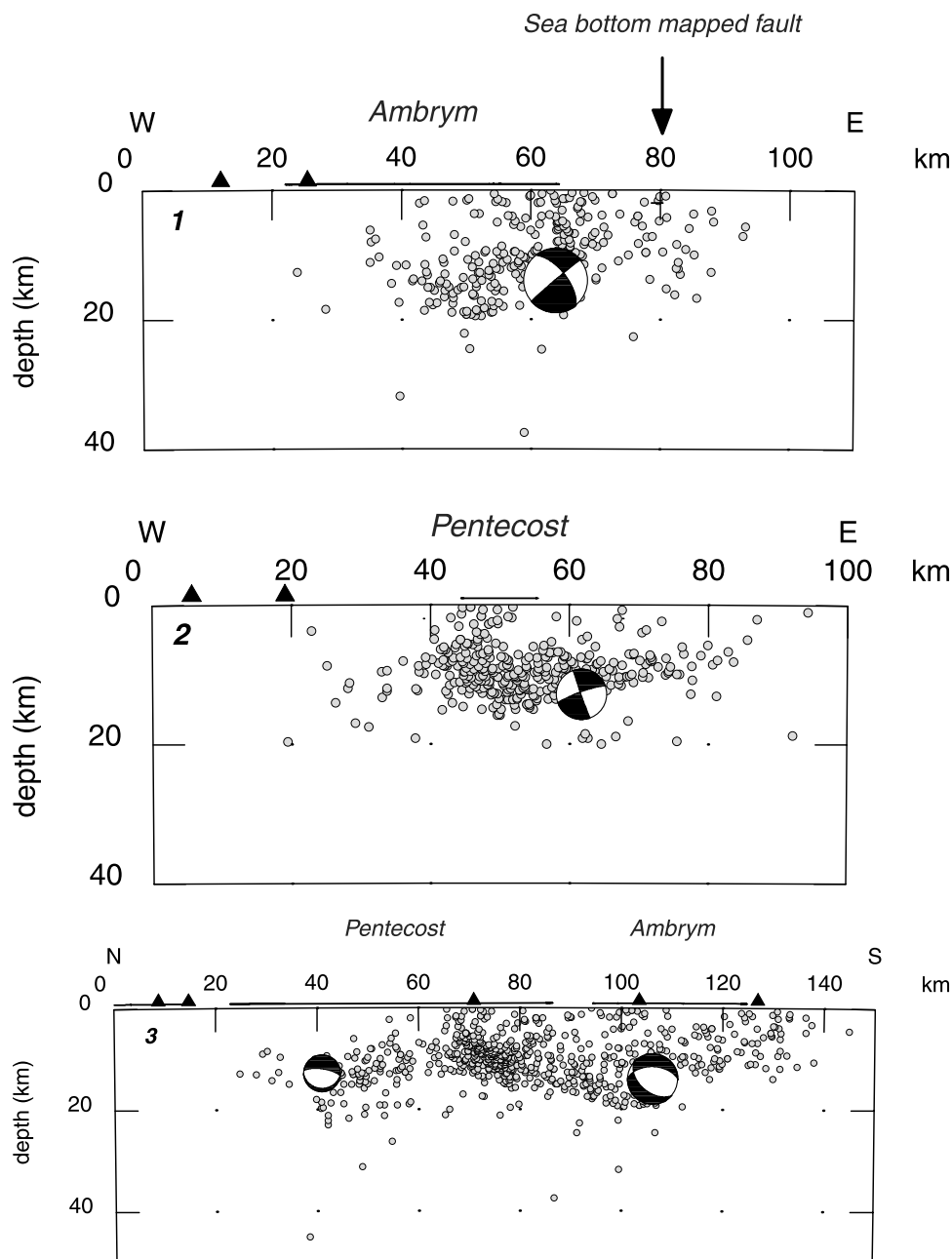


Figure 5. Cross sections 1 and 2 are oriented perpendicular to the strike of the fault plane ($N174^\circ$). The sea bottom scarp ($N165^\circ$) is indicated on the cross section 1. The main shock and largest aftershock focal mechanisms are plotted on their corresponding section. Cross section 3 is oriented parallel to the trend of the eastern belt. Islands and stations (triangles) positions are indicated on top of the section.

(1) a south dipping pattern beneath the southern half of Pentecost Island that merges with the scattered seismicity beneath Ambrym Island; and (2) a quite different seismic pattern, with no shallow seismicity, beneath the northern half of Pentecost Island and separated from the bulk of the aftershock zone by a small gap. These two features suggest Pentecost Island is divided into two blocks.

[12] The maximum depth reached by the seismicity is 20 km, in good agreement with the eastern belt crustal thickness determined by gravity and refraction studies

[Collot and Fisher, 1989; Pontoise et al., 1994]. This maximum depth of the seismicity images the lower boundary of the brittle domain, indicating no NFB crust has been underthrust beneath the Vanuatu arc crust.

6. GPS Data

[13] The IRD GPS network including the New Caledonia and Vanuatu archipelagoes on both sides of the New

Table 3. Coseismic Steps Observed by GPS

Site	Longitude, deg	Latitude, deg	Δ_{N-S} , mm	σ_{N-S} , mm	Δ_{E-W} , mm	σ_{E-W} , mm	Δ_{U-D} , mm	σ_{U-D} , mm
AMBR	167.924	-16.264	35	4	342	13	-41	8
AOBA	167.680	-15.419	-21	7	61	10	-42	14
AVNA	167.092	-15.643	1	2	39	5	3	7
BIGB	166.824	-15.156	7	10	20	21	-61	19
EKAR	167.059	-15.000	-19	7	27	8	-63	25
EMAE	168.375	-17.053	-12	10	9	14	-18	13
HOGB	167.103	-15.130	-9	4	32	8	-31	25
LISB	166.767	-15.631	4	9	28	6	-6	35
LMBU	167.393	-16.171	0	7	105	12	15	31
LVMP	167.240	-16.163	4	8	66	17	-14	13
MALO	167.247	-15.724	-5	6	61	10	-8	17
MAWO	168.078	-15.082	10	8	22	6	-26	11
MLKL	167.782	-16.451	46	7	115	11	0	17
NAMU	168.362	-16.831	-8	5	-6	5	-14	17
NEPI	168.162	-15.599	-48	9	22	20	-19	24
NSUP	167.403	-16.067	9	3	110	5	-3	6
NWST	166.545	-14.850	15	9	-3	6	-20	15
PNCT	168.156	-15.483	0	12	31	9	-37	13
RATA	167.090	-15.603	12	8	39	6	-21	11
RATU	167.188	-15.615	3	7	39	10	-5	16
RNSR	167.564	-16.213	6	3	124	6	0	6
SANC	167.203	-15.447	-3	1	39	2	-6	4
SWBY	167.446	-16.484	24	5	65	8	-6	9
TASM	166.903	-15.610	6	11	36	6	-5	11
TGOA	168.534	-16.917	5	6	0	5	-9	7
TNMR	167.174	-16.013	-7	8	73	6	-2	10
TSRK	166.780	-15.592	-13	6	44	8	-3	12
VMVS	167.382	-16.231	14	7	84	10	-19	11
VOTL	168.280	-16.803	-18	6	18	4	-38	9
WLRN	167.375	-15.990	-6	16	82	7	2	14
WUSI	166.661	-15.356	-8	7	4	7	-39	42

Hebrides trench started since 1990. This network of temporary sites is framed by six permanent stations (C-GPS), three in New Caledonia, two in Vanuatu (on Efate and Santo islands) and one in Futuna island. Observations on the temporary sites have been performed using dual-frequency receivers, mostly Ashtech Z12 and according choke ring antennae. Every site is observed at least once a year (more frequently in particular in case of earthquake). Observations last at least 3 GMT days. The GPS solutions are computed on the basis of daily sessions using the Bernese software [Rotacher *et al.*, 1993]. Extensive analysis of the processing is reported by Calmant *et al.* [2003].

[14] The crustal displacements related to the Ambrym event and analyzed in this paper only involve the Central Vanuatu subset of the GPS network which has been reoccupied shortly after the earthquake. The GPS-derived coseismic displacements are reported in Table 3. The largest horizontal offset (35 cm, trending eastward) is found at the western tip of Ambrym island (AMBR). Decimetric eastward offsets are found on Malekula island, west of Ambrym island. Offsets decrease northward up to a few centimeters on Malo, Santo, and Aoba islands. Small displacements are observed on Maewo and Pentecost islands and on Epi group islands, although close to the epicenter. Noteworthy, sites on Epi group islands show southward displacements. Vertical motions appear very scattered, in particular at Santo where large subsidences are derived for the northernmost sites. We interpret this scatter as the result of the dramatic

weather conditions of heavy rains suffered there during the survey undertaken after the quake, including an interruption of the field work because of the occurrence of a cyclone. The GPS-derived vertical offsets are then not used in this study.

7. Main Shock Fault Model

[15] A preliminary 80 km long fault model, striking $N191^\circ$ (from the initial Harvard CMT solution), for the Ambrym earthquake was proposed based on the total along-strike extension of the aftershock zone [Pelletier *et al.*, 2000]. However, the vertical motions computed with a dislocation model [Okada, 1985] using the revised Harvard focal solution (the fault plane strikes now at $N174^\circ$) and the 80 km long fault model are not compatible with observations of null or negative coseismic displacements inferred from biological markers analysis [Pelletier *et al.*, 2000] in the two areas to the north (Martelli bay and the eastern coast of south Pentecost) and south (the Paama and Lopevi Islands) of Ambrym island. These observations impose a maximum length of 50 km instead for the along-strike extension of the main shock fault (Figure 6), in agreement with the length of the corresponding segment of the sea bottom mapped scarp. Large coseismic vertical motions up to 1.2 m have been only observed on the easternmost part of Ambrym. The uplift decreases rapidly westward from 1.2 m to nil over a 3 km distance [see Pelletier *et al.*, 2000, Figure 4]. These measurements evidence a high east-west gradient of vertical motion that constrains the location of the western edge of the rupture zone beneath the eastern part of the island (Figure 6). The width of the fault is then relatively well constrained between the sea bottom scarp and the projection at depth of the vertical displacement nodal line. This crude estimate of the fault size, 50 km by 25 km, also corresponds to Ambrym island zone of weak aftershock activity (cross section 1 on Figure 5) where the main shock occurred.

[16] In order to further define the effective zone on the fault where most of the seismic moment was released, we inverted crustal coseismic motions measured from GPS data. The crustal displacements computed with a dislocation model [Okada, 1985] are compared to the data set made of both the GPS-derived horizontal displacements and field survey measurements of vertical motions. We have assumed a constant displacement over a rectangular rupture surface. We searched for the best fitting solution by a trial and error method. We used the mechanism established in this study and the geometry of the earthquake source constrained with the field survey data set as an initial model (Figure 6). We explored departures from this solution for the length and width of the fault, its central position, its azimuth and dip, and the rake of the slip vector on the fault plane. The set of parameter values best fitting the data set is summarized in Table 4. The fault is centered at $16.150^\circ S$ and $168.310^\circ E$. The length of the ruptured surface is 35 km long, slightly less than determined from the spread of the aftershocks. The width of the ruptured surface is 20 km and the central depth is

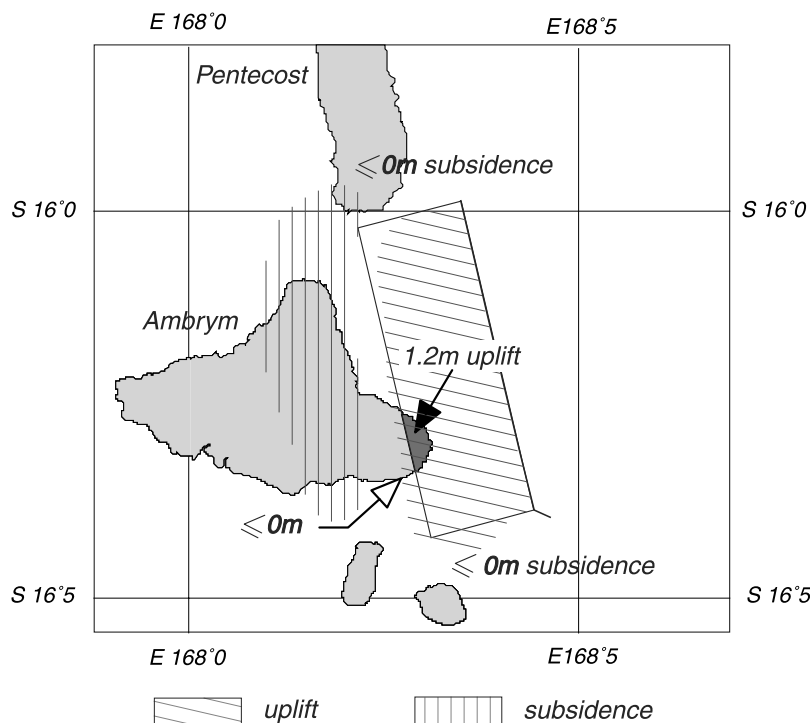


Figure 6. Map view of the Ambrym earthquake fault geometry estimated from the spatial distribution of the seismicity and from the vertical coseismic displacements inferred from biological markers observed along the coast of surrounding islands. Hatched zones show computed areas of uplift or subsidence using the fault dimensions shown ($50 \times 25 \text{ km}^2$) and the Harvard focal mechanism solution. Length and width of the fault are strongly constrained by the observation of nil uplift to the north, south, and west of the inferred fault.

8 km. According to this geometry and position, the rupture reached the surface. The best fitting geometry of the slip vector (Table 3) is obtained for a bearing fault oriented $N170^\circ$ and dipping 40° . The rake of the slip vector is 64° , which results in a slip vector pointing $N112^\circ$. Although slightly different from available focal mechanisms, these values remain globally consistent with seismological imaging of the fault. They suggest that most of the energy was released on a surface smaller than the whole activated surface, and which the barycenter is a few kilometers away from the first-motion hypocenter (the initial point of rupture), but quite close to the centroid hypocenter given by Harvard. With respect to that surface and the seismic moment of $1.67 \times 10^{27} \text{ dyn cm}$, a slip of 6.53 m and an elastic modulus μ of $0.35 \times 10^{12} \text{ dyn/cm}^2$ are found. The value of μ suggests that the faulting occurred in crustal material. This value is clearly a maximum value and remains much smaller than one would expect for faulting in a subduction context that is characterized by larger values of μ [e.g., *Ben-Menahem and Singh*, 1981]. Larger values of μ would induce too small displacements on the western belt. The crustal rheology and shallow depth of the main shock support the model of faulting occurring within the BATB crust in an intraplate thrusting context.

[17] Simulated horizontal displacements are reported in Figure 7 together with the GPS-derived horizontal offsets.

Simulated vertical motions on Ambrym and South Pentecost are reported in Figure 8. The large amount of slip assuming the rupture reached the seafloor is an important factor to explain the generation of the tsunami that followed the earthquake and reached on average a height of 3 m along the eastern coast of Ambrym island with localized run-up heights up to 7 m.

[18] It is worth noting that the GPS data set of horizontal motions over the group of islands surrounding the Aoba basin and the on-site observations of vertical motions on the eastern belt would be separately fitted by somewhat differ-

Table 4. Characteristics of the Fault and Slip Used to Simulate Coseismic Crustal Motions

Characteristic	Value
Position of the fault center	
Central longitude	168.310
Central latitude	-16.150
Central depth	7.5 km
Length	35 km
Width	20 km
Geometry of ruptured plane	
Azimuth	$N170^\circ$
Dip	40°
Rake	64°
Amount of slip	6.5 m

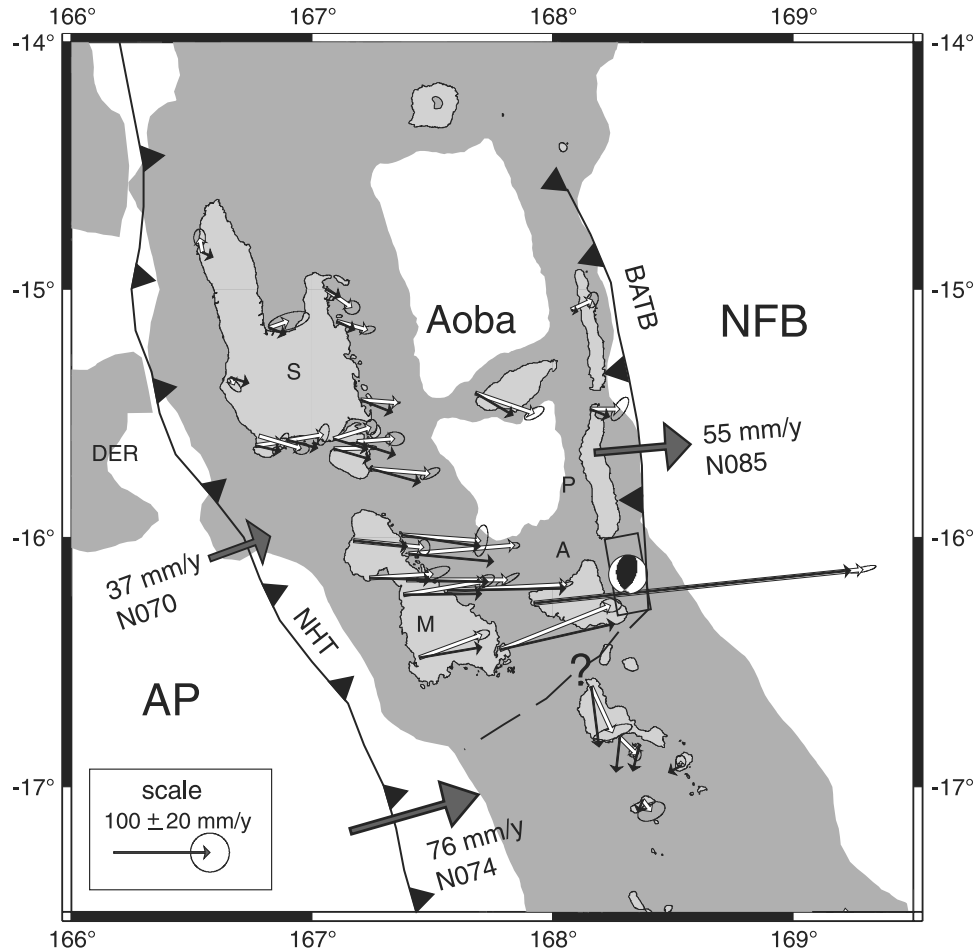


Figure 7. GPS-observed (white arrows) and simulated (black arrows) coseismic horizontal displacements. Ellipses are for 2σ uncertainties. The rectangle figures the surface projection of the fault. The dislocation parameters are figured according to the CMTS convention. See text and Table 4 for other parameters. Large gray arrows stand for the motion of relative convergence between the Australia plate and the Vanuatu platform on the left and between the Vanuatu platform and western North Fiji Basin on the right. See color version of this figure at back of this issue.

ent solutions. The strike of GPS vectors would be better modeled by a fault extending beneath South Pentecost. However, this implies that significant uplifts are modeled at South Pentecost, incompatible with on-site observations. Presumably, these differences reflect the difference between regional and near field deformation regime, the regional GPS deformations reflecting some average, integrated effect when the on-site observations, performed much closer to the fault reflect the nonuniformity of the rupture.

8. Stress Loading

[19] The two earthquake clusters located on Pentecost Island (Figure 4) are outside the rupture area of the derived fault model. Using the Harvard CMTS, static Coulomb stress changes resulting from slip of the main shock were computed to test whether the clusters of aftershocks located on the Pentecost occurred where the changes are positive.

We use the program GNStress version 1.5 available from R. Robinson [see, e.g., *Robinson and McGinty, 2000*] to compute the changes in Coulomb failure stress (CFS) at a depth of 10 km, the depth at which we observed the highest number of aftershocks, which is also very close to the depth of the main shock. The overall fit is satisfactorily with 80% of the aftershocks falling within areas of increased stresses (Figure 9). The largest cluster, located on the southern part of Pentecost falls within a large positive stress change due to the left-lateral strike-slip component of the focal mechanism (Figure 9). This zone of increased compressive stresses is also characterized by a permanent seismic gap. Then, the chances of occurrence of a moderate to large earthquake in this segment might have increased since the Ambrym events. The second cluster, further north, cannot be explain by the stress change pattern due to the main shock, but might be related to the largest aftershock (M_w 5.9) whose location, 15.60°S , 168.26°E , coincides with the cluster (Figure 4).

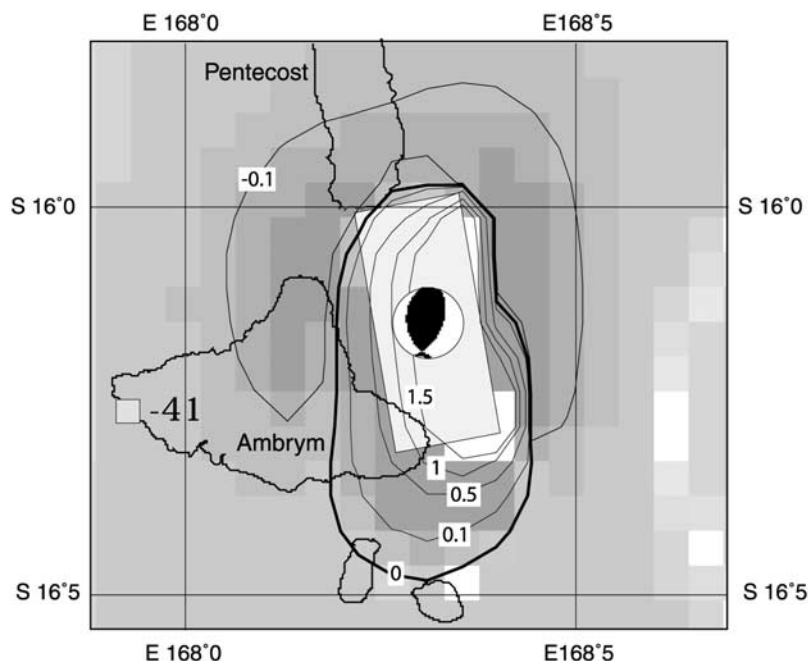


Figure 8. Simulated vertical motions. The rectangle figures the surface projection of the fault. The dislocation parameters are figured according to the CMTS convention. See text and Table 4 for other parameters. Isolines are -10 cm, 0 (bold), $+10$ cm, $+50$ cm, $+1$ m, $+1.5$ m, where plus and minus indicate areas of upward and downward, respectively, displacements. The number at west Ambrym site reports the GPS-derived vertical motions (in mm), not used to constrain the dislocation model. See color version of this figure at back of this issue.

[20] In the computations, we assume the rupture plane extends up to the seafloor, which is consistent with the observation of a fault scarp build up by accumulated offsets from repeated characteristic earthquakes. The computation of the changes in CFS at the surface shows a large area of decreases in CFS around the top of the fault plane in agreement with the very small number of aftershocks located in this area near the surface (Figure 5, cross section 1).

9. Spatiotemporal Distribution of the Seismic Activity

[21] On the cross section of Figure 10 are plotted events that occurred before (in dark gray) and after (in light gray) the main shock. The data set before the main shock covers a 2 year period (June 1997 to October 1999) but comes essentially from the 22 August 1999 earthquake sequence (Figure 2). Figure 10 shows there is little overlap between the zones defined by the seismic activity before and after the rupture. The main shock fault system (in light gray) appears to have been locked and the brittle deformations were concentrated eastward of it in the months preceding the main shock. Indeed foreshock activity clearly occurred in the footwall block at distances larger than 10 km from the main shock fault and its surface expression. Considering these distances are larger than the error on the hypocenters, we think the seismically imaged fault is a true feature resolved by the seismicity. This foreshock swarm defines a west

dipping plane in agreement with the fault plane chosen from the 22 August 1999 earthquake CMTS. During the Ambrym earthquake sequence, the easternmost plane of foreshock seismic activity (in dark gray) was quiescent while most of the accumulated stresses were released along the main fault plan and within the hanging wall block. Both transverse cross sections (Figure 11) support a model composed of several planes of seismicity rather than a simple volumetric distribution. These observations suggest that the eastern belt fault system is composed with several subparallel thrust fault reactivated during the Ambrym earthquake sequence.

10. Mode of Shortening

[22] The foreshock seismic zone also appears to be the easternmost seismically active area across the thrust belt. It is well correlated with very shallow crustal deformations observed in seismic lines and bathymetric data on the east side of the BATB, beyond the sea bottom mapped fault scarp (Lagabrielle et al., submitted manuscript, 2003). Considering that the age and amplitude of these deformations decrease eastward, the zone of foreshocks happens to be also the youngest deformed zone across the belt. The seismic activity located west of the main thrust (Figure 11) probably occurred on older fault that did not experienced significant slip as revealed by the analysis of coseismic displacements. This spatial distribution of faults across the belt seems to be organized with decreasing ages eastward

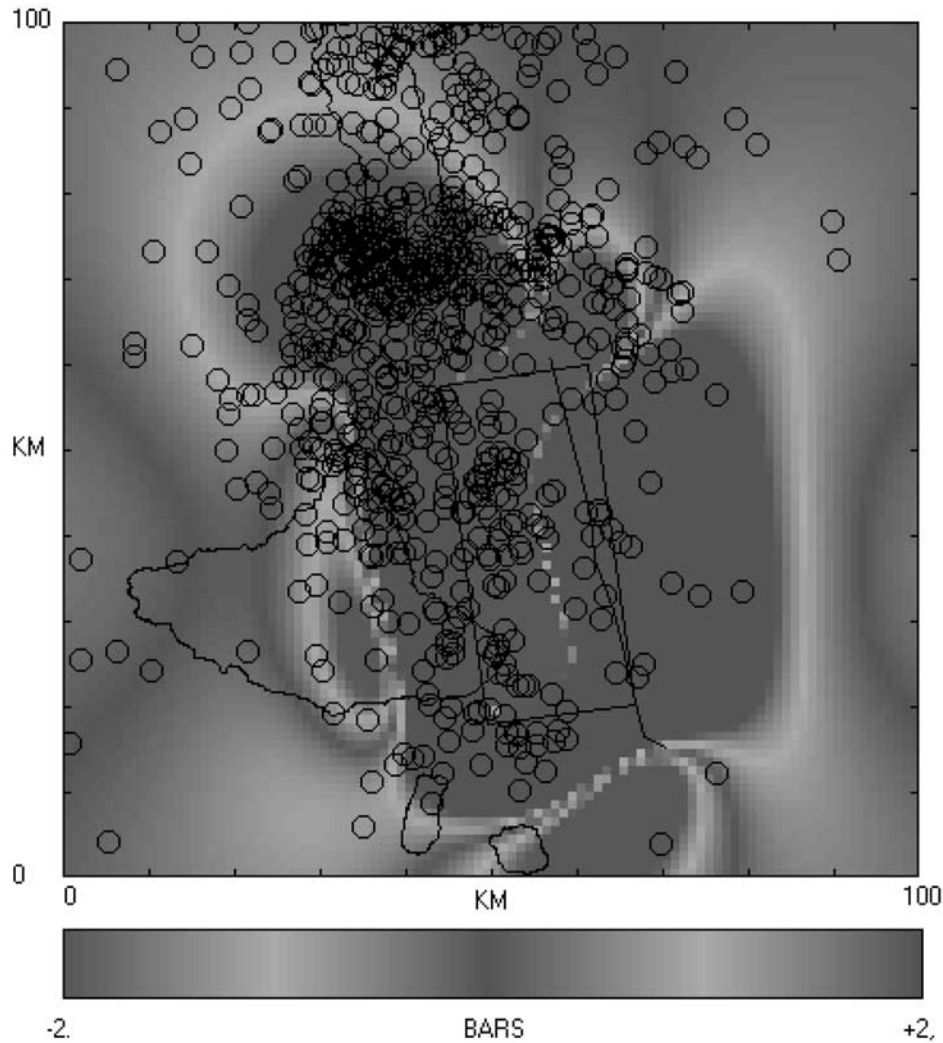


Figure 9. Coulomb stress changes (Δ CFS) at 10 km depth due to the Ambrym earthquake for optimally oriented faults. The rectangle is the surface projection of the fault plane. The sea bottom scarp is plotted as a black line close to the fault. Decreases in CFS occur in blue areas and increases in CFS occur in red areas. Circles indicate the aftershock epicenters. See color version of this figure at back of this issue.

and evidences that the back arc thrust belt forms in a forward thrusting sequence in a region under compressional regime caused by the convergence plate motion. New thrust faults develop eastward in the heading side of the main thrust in response to increasing strength across the present fault. In other words, the rupture along the present main fault will eventually occurs again until a new fault plane forms eastward by connecting smaller cracks into a single fault [Scholz, 1990]. The smaller slope and the abnormally large width of the foreshock seismic zone (Figure 10) support the model of an immature deformed zone that has not yet developed into a single throughgoing fault. This model yields to thrust belt building by slant stacking of oceanic thrust sheets.

[23] In this model, all the shortening observed between the eastern belt and the NFB resolved into thickening and

uplift of the back arc belt. The absence of magmatic addition to the eastern belt crust during the last 2 m.y. [Carney and Mac Farlane, 1982] and the simple almost linear convergence boundary along the eastern belt allow to use crustal balanced sections (2-D) to model recent deformations and estimate the cumulated shortening along the eastern belt boundary [Regnier *et al.*, 2001]. Figure 12 shows schematic cross sections of the eastern belt structure before and after shortening. Unfortunately there are almost no constraints on the crustal structure of the eastern belt before shortening. A 12 km thick NFB oceanic crust derived from the model of Pontoise *et al.* [1994] had been used in the modeling. The surface containing the earthquakes in the cross section on Figure 10 approximates the 20 km thick crustal domain of the present-day eastern belt. For computations all the crustal domains are decomposed in

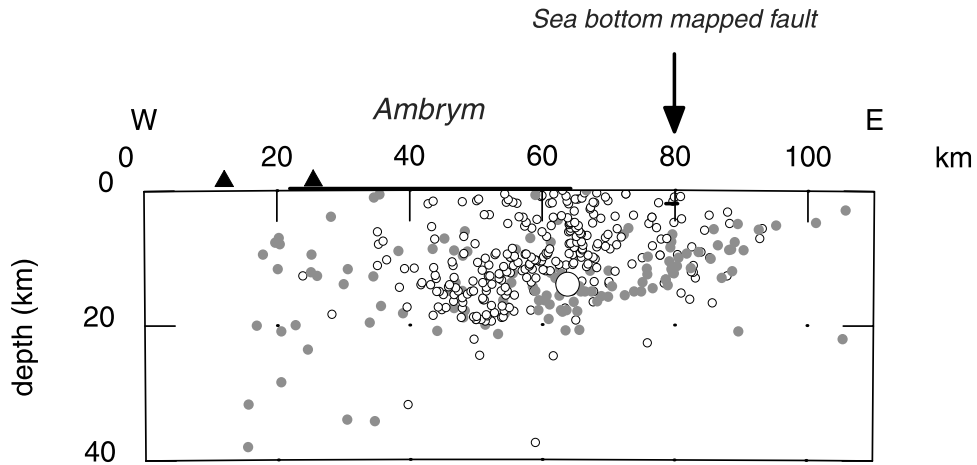


Figure 10. Migration of the seismicity located before (grey circles) and after the main shock (open circles) on a cross section oriented as the section 1 in Figure 5. The location of the Ambrym earthquake is represented with a large circle. The foreshock activity defines a plane that extends far beyond the sea bottom fault scarp, in a domain where recent seafloor deformations are observed.

simple geometrical shapes. In our model, only the NFB crust is stacked into a duplex like zone. A total shortening of 55 km is required to match the same area after deformation.

[24] If we assume the shortening occurred over a period of 1.8 m.y., since the d'Entrecasteaux ridge started to

subduct [Greene *et al.*, 1994], this yields an average shortening rate of 3 cm/yr. This is half the actual rate, but the assumption it has been constant all over the period is probably not realistic because the stress regime at the back arc has been controlled by the ongoing ridge-arc collision. Considering an initial null convergence rate along the back

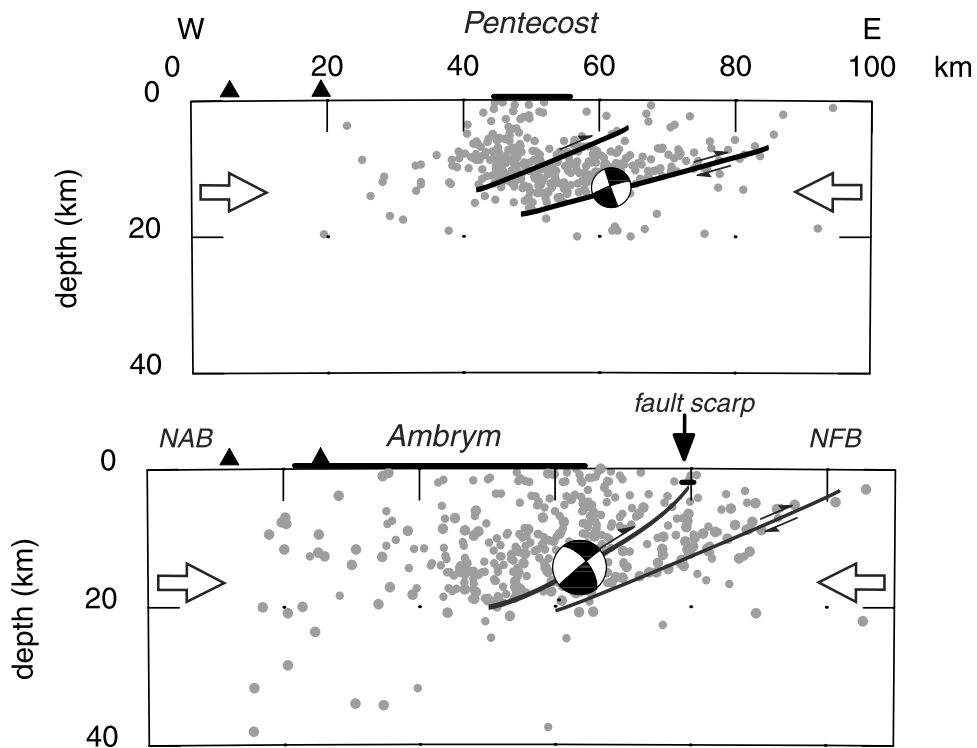


Figure 11. Structural interpretation of the back arc thrust belt beneath Pentecost and Ambrym island. White arrows indicate horizontal compressive stress.

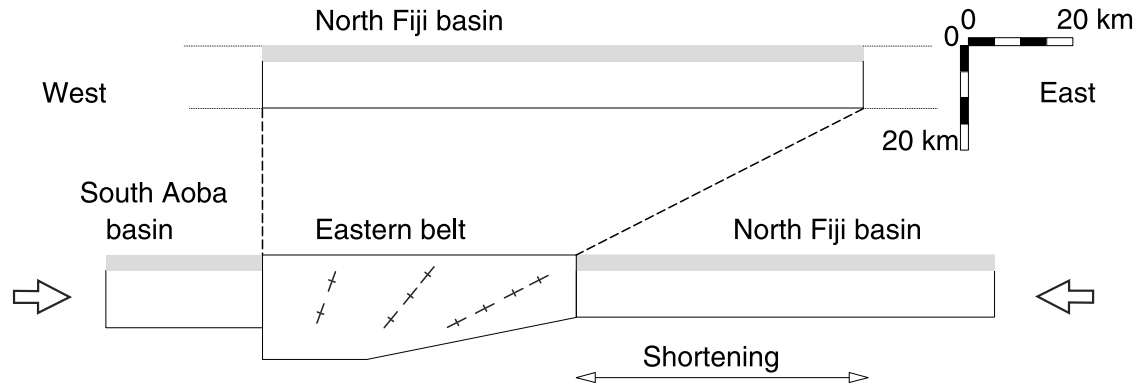


Figure 12. Schematic cross sections of the Eastern Belt and North Fiji Basin (top) before shortening started and (bottom) present. The water layer is in grey. Estimate of the cumulated shortening (55 km) is done using area balancing (2-D) before and after deformation up to now. The domain of seismic activity represents the present-day domain of the eastern belt. Schematic planes of seismicity indicate the duplex like structure of the belt.

arc and a linear increasing to a present measured convergence rate of 6 cm/yr [Calmant *et al.*, 2003], this implies a total shortening of 54 km, a value very similar to that obtained from area balancing. We can see this value as an upper bound for the total shortening. For a shorter period of deformation or for a thicker initial NFB or eastern belt crust, the cumulated shortening would be smaller.

11. Discussion

[25] The 26 November 1999 earthquake (M_w 7.5) took place in a region of moderate seismicity characterized by a seismic pattern made of alternating gaps and clusters along the eastern thrust belt (Figure 1). Together with the discontinuous morphology of the belt, this supports a model of an almost periodic segmentation of the belt. This segmentation is probably a mechanical response to the curved shape of the belt.

[26] The Ambrym earthquake fault has an estimated length of 50 km and spreads over the entire length of the Ambrym segment of the BATB. This indicates the rupture affected the whole Ambrym segment and therefore that the Ambrym earthquake is probably characteristic of this segment. The Ambrym 1999-type earthquakes in this segment may be responsible for the formation of the mapped seafloor scarp (500–900 m) built up by successive events, and for the distribution of uplifted flat reefs observed in cliffs along the eastern tip of Ambrym island (Lagabrielle *et al.*, submitted manuscript, 2003). Considering the fault of a magnitude M_w 7–7.5 earthquake has about the same length that the average segment length along the eastern belt (between 40 and 50 km), characteristic earthquakes with magnitudes in the range M_w 7–7.5 might occur in each segment. No large earthquake (magnitude > 7) have been reported or located in the twentieth century along the eastern belt except the November 1999 Ambrym event. This indicates a return period of more than 100 years for most of the thrust faults of the eastern belt.

[27] Our results show the main shock rupture did not occur in the easternmost zone of deformation where foreshock activity occurred, and confirm that a large magnitude earthquake, like the November 1999 Ambrym event, can only occur on a mature existing fault. This implies that seismic activity in the foreshock seismic zone is only related to recent small faults. The system of small faults can eventually grow into a single fault [Scholz, 1990] that will become the active main thrust fault, pushing forward the limit of the thrust front. This process yields a forward thrusting sequence along the eastern side of the BATB. Main consequences are continuous shortening along the boundary between the NFB and the BATB and thickening of the eastern belt crust. A typical model of subduction to accommodate the back arc convergence would not yield thickening which is required to explain the eastern belt morphology, with heights up to 900 m, and with a 20 km thick crust [Collot and Fisher, 1989]. Furthermore there is no seismic evidence of steady subduction zone along the BATB that would generate permanent seismic activity down to a depth of 27 km reached by a 55 km long, 30° dipping underthrust slab of NFB lithosphere. Rather, almost all of the seismicity is concentrated above a 20 km depth arguing for crustal thickening to accommodate back arc convergence. The few events with depths greater than 20 km on the Figure 5, section 1, have small magnitude (<4) and are located beneath the Ambrym volcano and are possibly related to a magmatic activity. By comparison, there is no deeper activity shown in section 2 (Figure 5) as there is no volcano at the latitudes (see Figure 4) sampled by this west-east cross section. Moreover all the CMTS from the cluster on Ambrym island (see on Figure 1) have estimated shallow depths as for the November 1999 main shock, confirming the absence of seismic moment release below the BATB crust during a period of 25 years in the intermediate and large magnitude range.

[28] A possible explanation to account for this model of back arc deformations is that the NFB plate is quite young

(12–10 Ma [Auzende *et al.*, 1995]) and has a high buoyancy that prevents it from penetrating easily into the Vanuatu arc lithosphere. Could this tectonic context be related to subduction initiation? The east margin of the BATB represents a zone of weakness where increasing horizontal stresses are accommodated into tectonic thickening. Because this type of convergence is energetically disadvantageous and therefore unstable as it evolves by a periodic failure of the whole crust, a new zone of subduction (with opposite polarity) can eventually develop along the main back arc thrust fault [Chemenda *et al.*, 1997]. The BATB present setting would then represent the very early stages of an incipient subduction with no slab or a very little length of a slab penetrating into the lithosphere. The lack of seismicity beneath the BATB crust is interpreted as the absence of a slab but the subduction of a small amount of NFB plate into the lithosphere could eventually appear aseismic as it happens into a ductile domain. The data used in this study can not actually resolve this alternative.

[29] Our results show the rupture zone determined from aftershocks distribution is relatively small ($50 \times 25 \text{ km}^2$). A

smaller surface ($35 \times 20 \text{ km}^2$) is found from geodetical data with an average slip of 6.5 m. This difference indicates a non uniform slip on the rupture zone. The slip value remains a very high value for a magnitude 7.5 earthquake. If we calculate the stress drop using a circular crack model and with $M_0 = 1.6 \times 10^{20} \text{ N m}$, we obtain an estimate of 178 bars for the small rupture zone or 92 bars for the larger, which are both high values of stress drop. High stress drop above 100 bars are usually typical of intraplate earthquakes [Kanamori and Anderson, 1975] and are also associated with long recurrence time [Kanamori and Allen, 1986]. These calculations are consistent with our model of an intraplate earthquake for the Ambrym event.

[30] **Acknowledgments.** We thank Jean Philippe Caminade, Sophie Jimmykone, and David Nakedau for running the local seismic network in Vanuatu, Jean Michel Bore and Jean Claude Willy for acquiring the GPS data. We thank Russell Robinson of the IGNS in New Zealand for providing his program GNStress. We thank Serge Lallemand and Trevor Jones for suggestions that improved this manuscript. This work has been supported by IRD (formerly ORSTOM). Geoscience Azur contribution 562.

References

- Auzende, J. M., B. Pelletier, and J.-P. Eissen, The North Fiji Basin: Geology, structure and geodynamic evolution, in *Back-Arc Basin: Tectonics and Magmatism*, edited by B. Taylor, pp. 175–195, Plenum, New York, 1995.
- Ben-Menahem, A., and S. J. Singh, *Seismic Waves and Sources*, Springer-Verlag, New York, 1981.
- Calmant, S., P. Lebellegard, F. W. Taylor, M. Bevis, D. Maillard, J. Recy, and J. Bonneau, Geodetic measurements of convergence across the New Hebrides subduction zone, *Geophys. Res. Lett.*, **22**, 2573–2576, 1995.
- Calmant, S., B. Pelletier, P. Lebellegard, M. Bevis, F. W. Taylor, and D. A. Phillips, New insights on the tectonics along the New Hebrides subduction zone based on GPS results, *J. Geophys. Res.*, **108**(B6), 2319, doi:10.1029/2001JB000644, 2003.
- Carney, J. N., and A. Mac Farlane, Geological evidence bearing on the Miocene to Recent structural evolution of the New Hebrides arc, *Tectonophysics*, **87**, 147–175, 1982.
- Chemenda, A. I., P. Matte, and V. Sokolov, A model of Paleozoic obduction and exhumation of high-pressure/low-temperature rocks in southern Urals, *Tectonophysics*, **276**, 217–227, 1997.
- Collot, J.-Y., and M. A. Fisher, Crustal structure, from gravity data, of a collision zone in the central New Hebrides island arc, in *Geology and Offshore Resources of Pacific Islands Arcs-Vanuatu Region*, *Earth Sci. Ser.*, vol. 8, edited by H. G. Greene and F. L. Wong, pp. 125–139, Circum-Pac. Council for Energy and Miner. Resour., Houston, Tex., 1989.
- Collot, J.-Y., J. Daniel, and R. V. Burne, Recent tectonics associated with the subduction/collision of the D'Entrecasteaux zone in the central New Hebrides, *Tectonophysics*, **112**, 325–356, 1985.
- Frohlich, C., M. F. Coffin, C. Massell, P. Mann, C. L. Schuur, S. D. Davis, T. Jones, and G. Karner, Constraints on Macquarie Ridges tectonics provided by Harvard focal mechanisms and teleseismic earthquake locations, *J. Geophys. Res.*, **102**, 5029–5041, 1997.
- Greene, H. G., et al., *Proceedings of the Ocean Drilling Program, Scientific Results*, vol. 134, 665 pp., Ocean Drill. Program, College Station, Tex., 1994.
- Kanamori, H., and C. A. Allen, Earthquake repeat time and average stress drop, in *Earthquake Source Mechanics*, *Geophys. Monogr. Ser.*, vol. 37, edited by S. Das et al., pp. 227–235, AGU, Washington, D. C., 1986.
- Kanamori, H., and D. L. Anderson, Theoretical basis of some empirical relations in seismology, *Bull. Seismol. Soc. Am.*, **65**, 1073–1095, 1975.
- Kikuchi, M., and H. Kanamori, Inversion of complex body waves-III, *Bull. Seismol. Soc. Am.*, **81**, 2335–2350, 1991.
- Louat, R., and B. Pelletier, Seismotectonics and present day relative plate motions in the New Hebrides-North Fiji Basin region, *Tectonophysics*, **167**, 41–55, 1989.
- Nabeleck, J., Determination of earthquake fault parameters from inversion of body waves, Ph.D. thesis, 361 pp., Mass. Inst. of Technol., Cambridge, 1984.
- Okada, Y., Surface displacement due to shear and tensile faults in a half-space, *Bull. Seismol. Soc. Am.*, **75**, 1135–1154, 1985.
- Pelletier, B., M. Meschede, T. Chabernaud, R. Roperch, and X. Zhao, Tectonics of the central New Hebrides arc, North Aoba basin, *Proc. Ocean Drill. Program Sci. Results*, **134**, 431–444, 1994.
- Pelletier, B., S. Calmant, and R. Pillet, Current tectonics of the Tonga-New Hebrides region, *Earth Planet. Sci. Lett.*, **164**, 263–276, 1998.
- Pelletier, B., et al., Le séisme d'Ambrym-Pentecôte (Vanuatu) du 26 novembre 1999 (M_w 7.5), Données préliminaires sur la sismicité, le tsunami et les déplacements associés, *C. R. Acad. Sci., Ser. II*, **331**, 21–28, 2000.
- Pillet, R., M. Regnier, S. Calmant, B. Pelletier, J. M. Bore, J. P. Caminade, C. Ioan, and S. Temakon, The M_w 7.5 November 26, 1999 Ambrym earthquake, a major event in the central New Hebrides back arc, Vanuatu, paper presented at SSA Meeting, Seismol. Soc. of Am., San Diego, Calif., April 2000.
- Pontoise, B., C. Charvis, and M. Gérard, Sedimentary and crustal structure of the North Aoba Basin from seismic refraction data, *Proc. Ocean Drill. Program Sci. Results*, **134**, 459–563, 1994.
- Regnier, M., B. Pelletier, R. Pillet, S. Calmant, Y. Lagabrielle, J.-P. Caminade, and J.-M. Bore, Fault characteristics of the M_w 7.5 November 26, 1999, Ambrym earthquake, Vanuatu, paper presented at EGS Meeting, Eur. Geophys. Soc., Nice, France, April 2001.
- Robinson, R., and P. McGinty, The enigma of the Arthur Pass, New Zealand earthquake: 2. The aftershock distribution and its relation to regional and induced stress, *J. Geophys. Res.*, **105**, 16,139–16,150, 2000.
- Rotacher, M., G. Beutler, W. Gurtner, E. Brockman, and L. Nervart, Documentation for Bernese GPS Software version 3. 4, Univ. of Bern, Bern, Switzerland, 1993.
- Scholz, C. H., *The Mechanics of Earthquakes and Faulting*, Cambridge Univ. Press, New York, 1990.
- Smith, G. P., and G. Ekstrom, Interpretation of earthquake epicentre and CMT centroid locations, in terms of rupture length and direction, *Phys. Earth Planet. Inter.*, **102**, 123–132, 1997.
- Taylor, F. W., C. Frohlich, J. Lecolle, and M. Strecker, Analysis of partially emerged corals and reef terraces in the central Vanuatu arc: Comparison of contemporary coseismic and nonseismic with Quaternary vertical movements, *J. Geophys. Res.*, **92**, 4905–4933, 1987.
- Taylor, F. W., et al., Geodetic measurements of convergence at the New Hebrides island arc indicate arc fragmentation caused by an impinging aseismic ridge, *Geology*, **23**, 1011–1014, 1995.
- S. Calmant, Y. Lagabrielle, B. Pelletier, and M. Regnier, UR082/UMR Géosciences Azur, IRD, BP A5 Nouméa, New Caledonia. (regnier@noumea.ird.nc)
- G. Cabioch, UR055 “Paléotropical”, IRD, BP A5 Nouméa, New Caledonia.

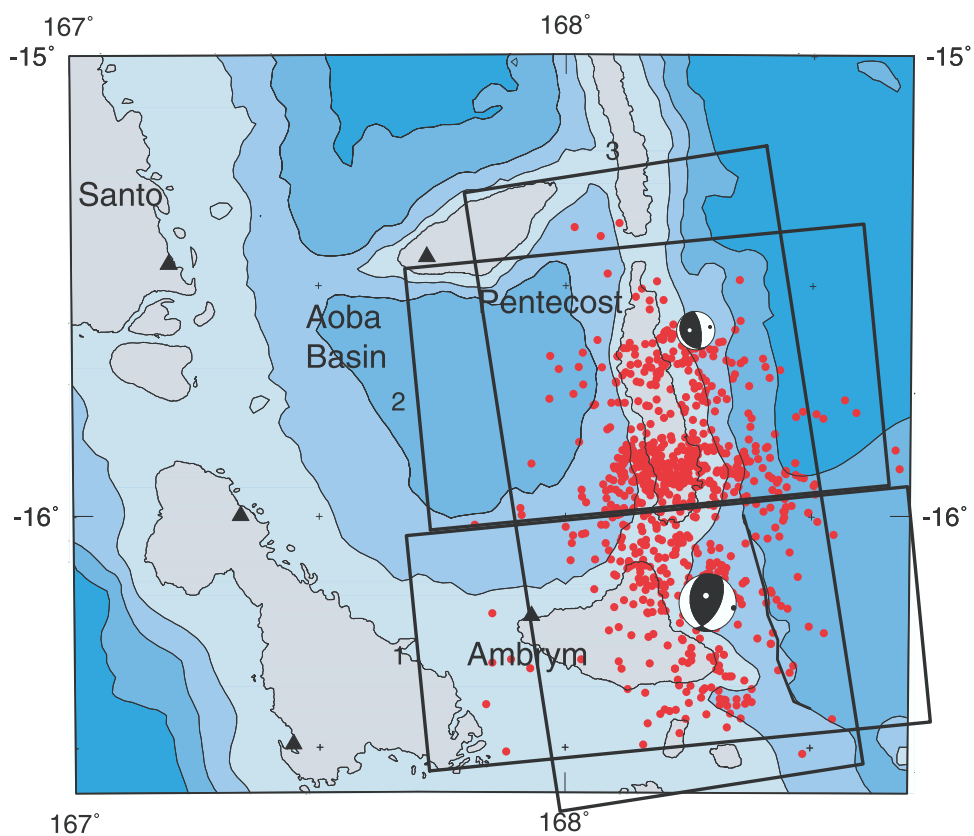


Figure 4. Map of shallow epicenters (depth < 30 km) for a 7 month period after the main shock. The locations of the cross sections are reported. The mapped seafloor scarp is plotted as a black line east of the main shock around the isobaths 2000 m.

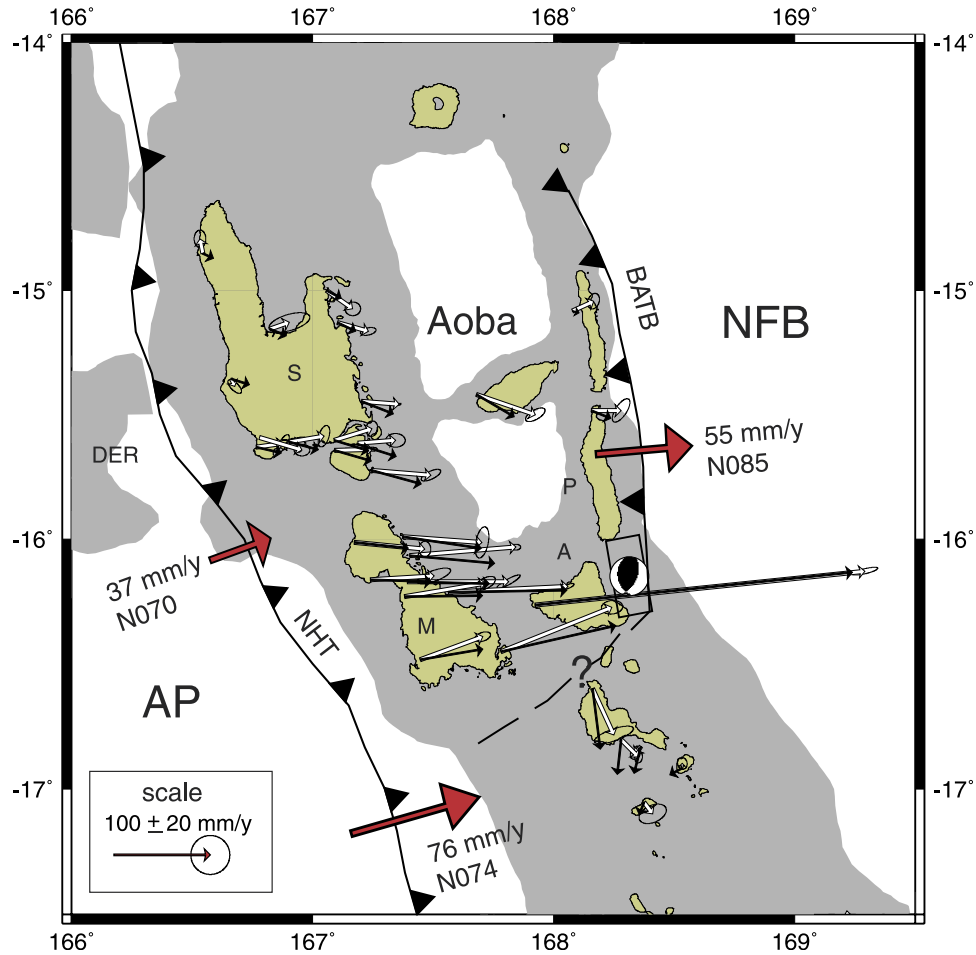


Figure 7. GPS-observed (white arrows) and simulated (black arrows) coseismic horizontal displacements. Ellipses are for 2σ uncertainties. The rectangle figures the surface projection of the fault. The dislocation parameters are figured according to the CMTS convention. See text and Table 4 for other parameters. Large gray arrows stand for the motion of relative convergence between the Australia plate and the Vanuatu platform on the left and between the Vanuatu platform and western North Fiji Basin on the right.

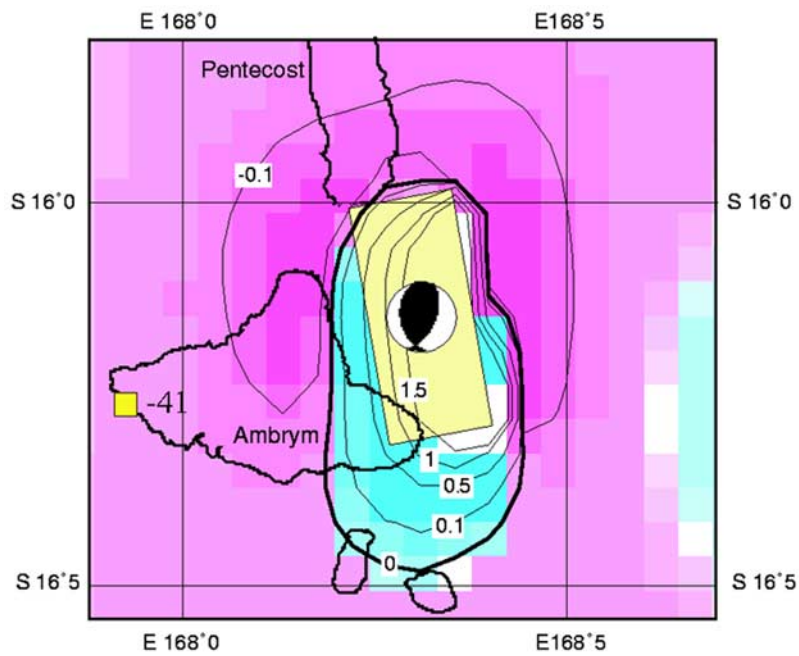


Figure 8. Simulated vertical motions. The rectangle figures the surface projection of the fault. The dislocation parameters are figured according to the CMTS convention. See text and Table 4 for other parameters. Isolines are -10 cm, 0 (bold), $+10$ cm, $+50$ cm, $+1$ m, $+1.5$ m, where plus and minus indicate areas of upward and downward, respectively, displacements. The number at west Ambrym site reports the GPS-derived vertical motions (in mm), not used to constrain the dislocation model.

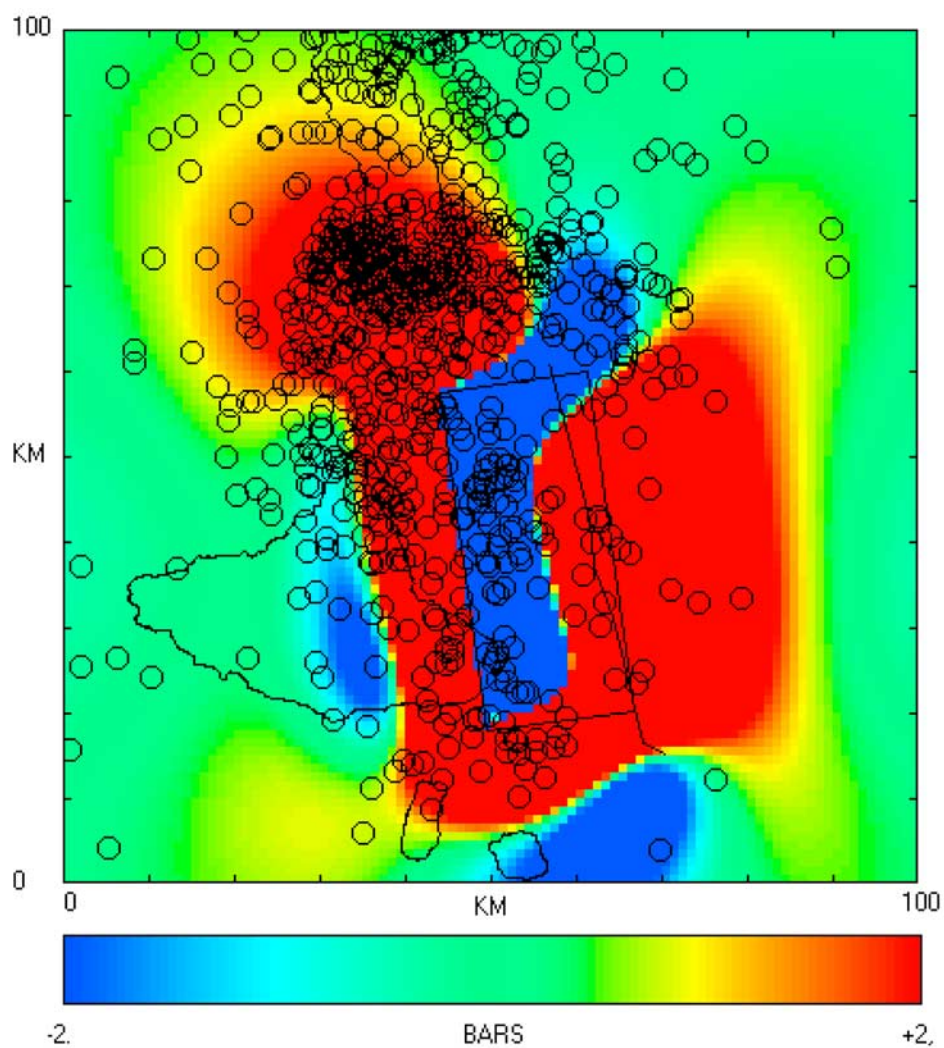


Figure 9. Coulomb stress changes (Δ CFS) at 10 km depth due to the Ambrym earthquake for optimally oriented faults. The rectangle is the surface projection of the fault plane. The sea bottom scarp is plotted as a black line close to the fault. Decreases in CFS occur in blue areas and increases in CFS occur in red areas. Circles indicate the aftershock epicenters.